Pion Energy Reconstruction by the Local Hadronic Calibration Method with ATLAS Combined Test Beam 2004 data

Y.Kulchitsky, P.Tsiareshka

JINR, Dubna, Russia &
IP National Academy of Sciences, Minsk, Belarus

J.Khubua, N.Russakovich, V.Shigaev, V.Vinogradov

JINR, Dubna, Russia

Abstract

The pion energy reconstruction by the local hadronic calibration method on the basis of the 2004 combined test beam data in the energy range 10 – 350 GeV and $\eta = 0.25$ is performed. In this method energies deposited in each cell are weighted. The weights are determined by the Monte Carlo simulation using Calibration Hits software. We have modified this method by applying cuts in weights. The obtained fractional energy resolution with the conventional method of determination of the energy deposit in the dead material between LAr and Tile calorimeters is $\sigma/E = (67 \pm 2)\%/\sqrt{E} \oplus (3.9 \pm 0.2)\% \oplus (95 \pm 22)\%/E$. This is about 1.5 times better than the results for the hadronic calibration method obtained by the Oxford-Stockholm group and slightly better than the H1 method results for CTB04 obtained by Pisa group. The energy linearity is within $\pm 1\%$. We have determined the general normalization constant of 0.91 for which the mean value linearity for the weight cut of 1.05 is about 1. At using this normalization constant the energy resolution has not worsen. We have corrected the cesium miscalibration of the $Tile_1$ and $Tile_2$ longitudinal samplings. The mean value of energy linearity has been increased by about 1% and becomes equal to 1.002 ± 0.002. The energy resolution did not change. We have performed weighting without knowing of the beam energies. For this the special procedure has been developed. In this case the energy resolution shows 9% degradation. Linearities are within $\pm 1\%$. We have applied the Neural Networks to the determination of the energy deposit between LAr and Tile calorimeters. The essential improvement of energy resolution is obtained. In this case we have reached the projected energy resolution for hadrons in the ATLAS detector $\sigma/E = 50\%/\sqrt{E} \oplus 3\%$.

1 Introduction

The constructed ATLAS detector at the LHC will have the great physics discovery potential, in particular in the detection of a heavy Higgs boson [1, 2]. Calorimeters will play a crucial role in this. The key question of calorimetry is the energy resolution.

The physics goals have led to the following requirement for the energy resolution: in the case of hadronic jets the energy resolution should be the following [3]:

$$\frac{\sigma}{E} = \frac{50\%}{\sqrt{E}} \oplus 3\%. \tag{1}$$

In the year 2004, a huge combined test beam (CTB04) in the H8 channel of the SPS CERN has been fulfilled. A complete slice of the ATLAS barrel detector has been exposed by beams of different particles (pions, electrons, protons, muons and photons) at different energies and polarities, ranging from 1 GeV up to 350 GeV. A lot of data (90 million events, 4.6 TByte) has been collected for analysis. Unique opportunity to study the detector performance in the realistic combined data taking and to understand better the detector has been provided.

As to the hadronic calorimeters the following main purposes have been put:

- hadronic energy calibration [4],
- non-compensation (e/h) measurements,
- linearity and uniformity versus energy and η,
- shower containment and profiles,
- studies of energy losses in passive material (for example, cryostat walls),
- single particle and jet reconstruction [5].

In [6] a new weighting method for energy reconstruction has been suggested. This method reconstructs the energy in each cell of the calorimeter hit by the hadronic shower. The break up of nuclei, invisible energy, strongly reduces the detectable energy. It has to be compensated by weighting. Lately this method is called as the Local Hadronic Calibration Method [7, 8, 9].

Our work is devoted to Pion Energy Reconstruction on the CTB04 data by the Local Hadronic Calibration Method.

2 The combined testbeam setup

The testbeam setup shown in Figs. 1, 2 resembled the geometry and setup of the full ATLAS detector as much as was technically possible [5].

The beam particles hit the pixel and SCT modules, and then continue towards the TRT, the calorimeters and muon modules. The electromagnetic calorimeter prototype module (LAr) was housed inside a cryostat filled with liquid argon. For the hadron Tile calorimeter three barrel modules and three extended barrel modules were used. The Tile calorimeter modules were on a movable table that allows their rotation and translation, to simulate particles impinging at different pseudorapidities [10]. Upstream of the beam, before the pixel detector, there was a set of beam detectors that can be used to select the beam direction and to reject particles distant from the beam axis. Three plastic scintillators were used in coincidence to obtain the particle trigger. A scintillator placed downstream the Tile Calorimeter (MuTag in the following analysis) can be used to reject muons.

3 The Local Hadronic Calibration Method

3.1 Energy reconstruction

In this method in application to the CTB04 data the reconstructed energy on the hadronic scale is given by the expression:

$$E_{rec,\ had} = E_{LAr} + E_{Tile} + E_{dm} + E_{leak}, \tag{2}$$

where E_{LAr} is the energy deposition in the electromagnetic LAr calorimeter,

$$E_{LAr} = E_{LAr_0} + E_{LAr_1} + E_{LAr_2} + E_{LAr_3}, \tag{3}$$

E_{Tile} is the one in the hadronic Tile calorimeter

$$E_{Tile} = E_{Tile_0} + E_{Tile_1} + E_{Tile_2}, \tag{4}$$

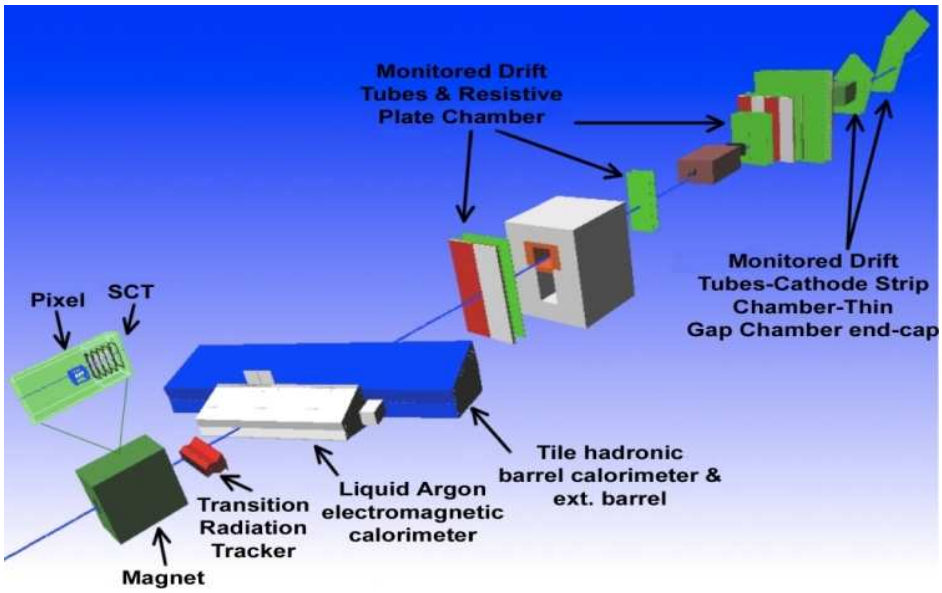

Figure 1: Geant4 Layout of the Combined Test Beam setup.

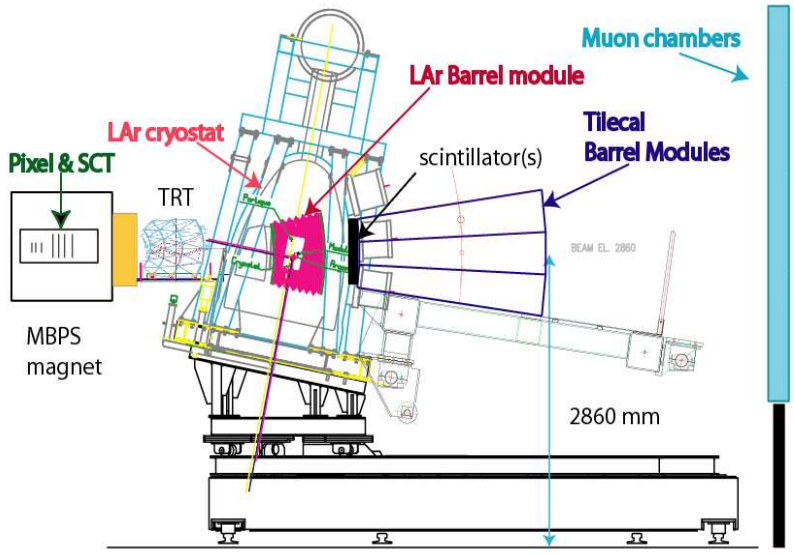

Figure 2: Schematic of the Combined 2004 Test Beam setup.

E_{dm} is the energy deposition in the dead material, E_{leak} is the energy leakage from the calorimeter. In each longitudinal sampling (E_{LAr_1}, E_{LAr_2}, E_{LAr_3}, $E_{Tile_0}, E_{Tile_1}, E_{Tile_2}$) the reconstructed energy is

$$E_{sampling} = \sum E^{cell}_{corr}, \tag{5}$$

where the sum runs over all calorimeter sampling cells. The value E^{cell}_{corr} is the corrected energy in each cell

$$E^{cell}_{corr} = w \cdot E^{cell}_{rec}. \tag{6}$$

The weights w are determined by the Monte Carlo simulation and are the ratios of true energy to reconstructed energy in cell on the electromagnetic scale [7]

$$w = E^{cell}_{truth}/E^{cell}_{rec,\ em}. \tag{7}$$

These weights allow to convert the experimental detected energy deposition on the electromagnetic scale into the real deposited energy in the hadronic scale. The weight is a function of an incident energy E_{inc}, longitudinal sampling and the energy density, ρ:

$$w = f(E_{inc},\ sampling,\ \rho), \tag{8}$$

where

$$\rho = E^{cell}_{rec,\ em}/Volume_{\ cell}. \tag{9}$$

3.2 Dead material and leakage corrections

We have parameterized the dead material and leakage corrections by the following way. The energy deposition before the calorimeter registered by presampler, E_{LAr_0}, is

$$E_{bef-LAr_0} = p_1(E_{rec,\ had}) \cdot E_{LAr_0}, \tag{10}$$

the one between E_{LAr_0} and E_{LAr_1} is

$$E_{LAr_0-LAr_1} = p_2 + p_3(E_{rec,\ had}) \cdot \sqrt{E_{LAr_0} \cdot E_{LAr_1}}, \tag{11}$$

the one between the LAr and Tile calorimeters is

$$E_{LAr-Tile} = p_4 \cdot \sqrt{E_{LAr_3} \cdot E_{Tile_0}}. \tag{12}$$

The energy leakage is

$$E_{leak} = p_5(E_{rec,\ had}) \cdot E_{rec,\ had}. \tag{13}$$

Figs. 3 – 4 show the relative energy depositions as a function of E_{beam} obtained by the Monte Carlo simulation. By approximation these points by the functions (10) – (13) we have determined the following parameterizations:

$$E_{bef-LAr_0} = (1.614 - 0.000675 E_{rec,\ had}) \cdot E_{LAr_0}, \tag{14}$$

$$E_{LAr_0-LAr_1} = 0.260 + (0.331 - 0.000104 \cdot E_{rec,\ had}) \cdot \sqrt{E_{LAr_0} E_{LAr_1}}, \tag{15}$$

$$E_{leak} = (0.0101 - 0.00522 \cdot \ln E_{rec,\ had} + 0.000792 \cdot \ln^2 E_{rec,\ had}) \cdot E_{rec,\ had}. \tag{16}$$

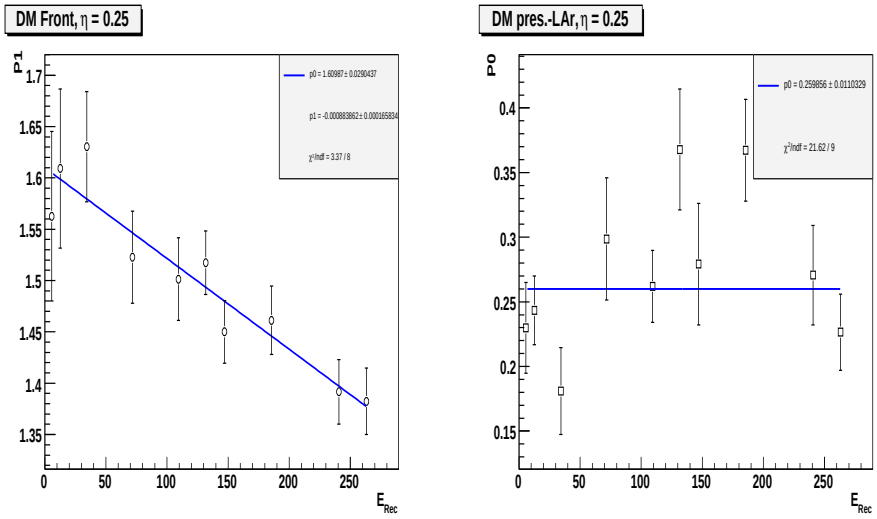

Figure 3: The dependencies of the parameter $p_1(E_{rec,\ had})$ for the energy depositions before the calorimeter (left) and the p_2 coefficient for the energy depositions (11) between the LAr_0 and LAr_1 samplings.

The p_4 coefficient in the formula (12) have been determined from Fig. 5 and equal of 1.52 for $\eta = 0.25$.

Fig. 6 shows the relative contributions of the various dead material and leakage corrections. The largest contribution, about 90%, comes from a region between the LAr and Tile calorimeters.

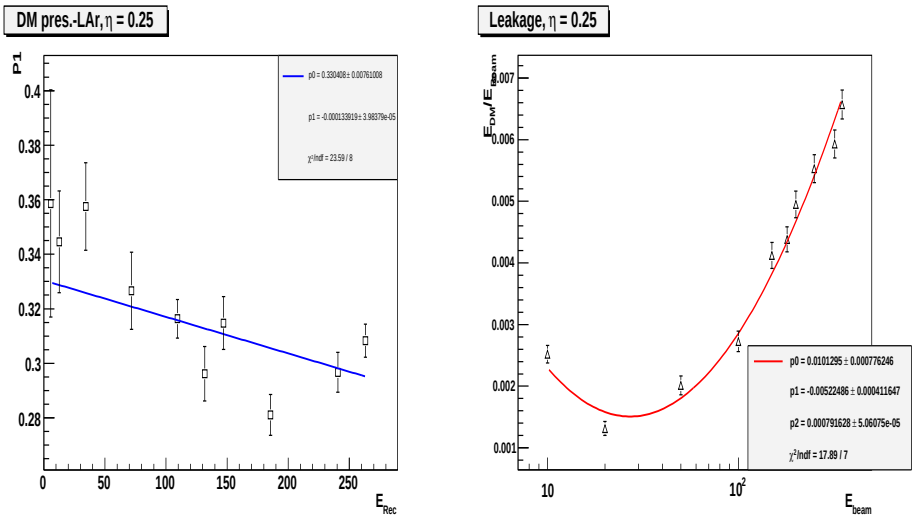

Figure 4: The energy dependence of the parameter $p_3(E_{rec,\ had})$ for the energy depositions (11) between the LAr_0 and LAr_1 samplings (left) and the relative leakage dependence, $p_5(E_{rec,\ had})$, (right).

The reconstructed energy, $E_{rec,\ had}$, used in the formulas (14) – (16), is determined by the iteration procedure

$$E_{rec,\ had,\ i+1} = E_{LAr} + E_{Tile} + E_{dm,\ i} + E_{leak,\ i}. \tag{17}$$

The input value

$$E_{rec,\ had,\ 1} = E_{LAr} + E_{Tile}. \tag{18}$$

The fulfilment of the condition

$$\mid (E_{rec,\ had,\ i+1} - E_{rec,\ had,\ i})/E_{rec,\ had,\ i} \mid < 0.001 \tag{19}$$

is required. Procedure is converged after 2 iterations.

4 Experimental Data

The data used in the present analysis are the Combined 2004 Test Beam Data at energies E = 10, 20, 50, 100, 150, 180, 200, 250, 350 GeV at $\eta = 0.25$. For each energy 10000 events have been analysed.

We have used the Athena release 12.0.31 and 4/2/0 CaloTopoCluster [7, 11, 12].

We have used the following selection criteria:

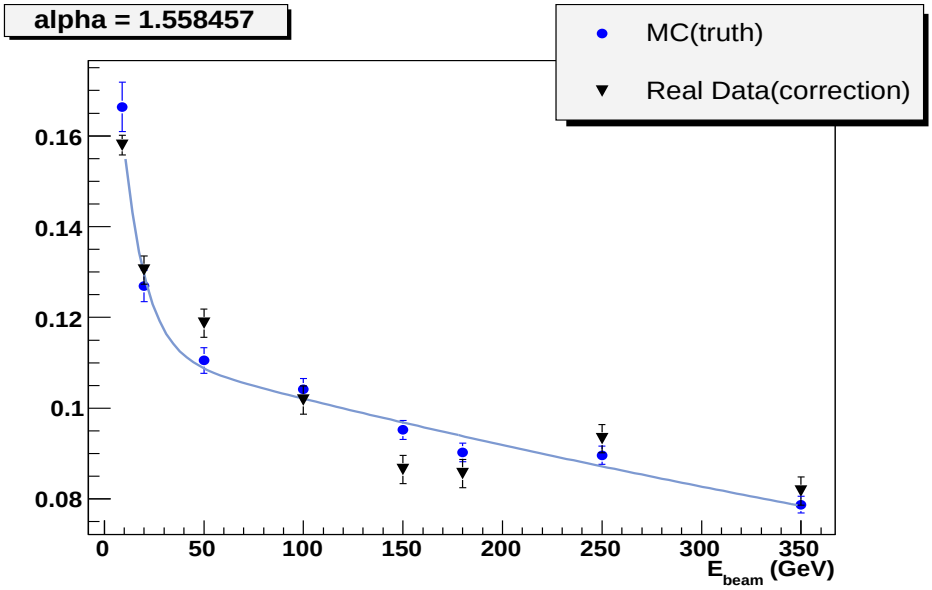

Figure 5: The mean relative Monte Carlo values (circles) and the values calculated by formula (12) (triangles) for LAr-Tile region as a function of beam energy.

1. muons removal from the incident particles, $MuTag < 500$,
2. electrons removal, $E_{Tile}/E_{beam} > 0.03$,
3. beam space restriction:
   (a) $Xcha1_{min} \leq Xcha1 \leq Xcha1_{max}$,
   (b) $Xcha2_{min} \leq Xcha2 \leq Xcha2_{max}$,
4. noise suppression, $E^{cell}_{reco} \geq 2\sigma_{noise}$ [7].

5 Monte Carlo simulation

For the Monte Carlo simulation we have used the Athena release 12.0.6, 4/2/0 CaloTopoCluster, 20000 events for each energy, Physics List QGSP_GN. We have used the calibration hits which allowed to have four types of energy deposition in each cell: electromagnetic energy,

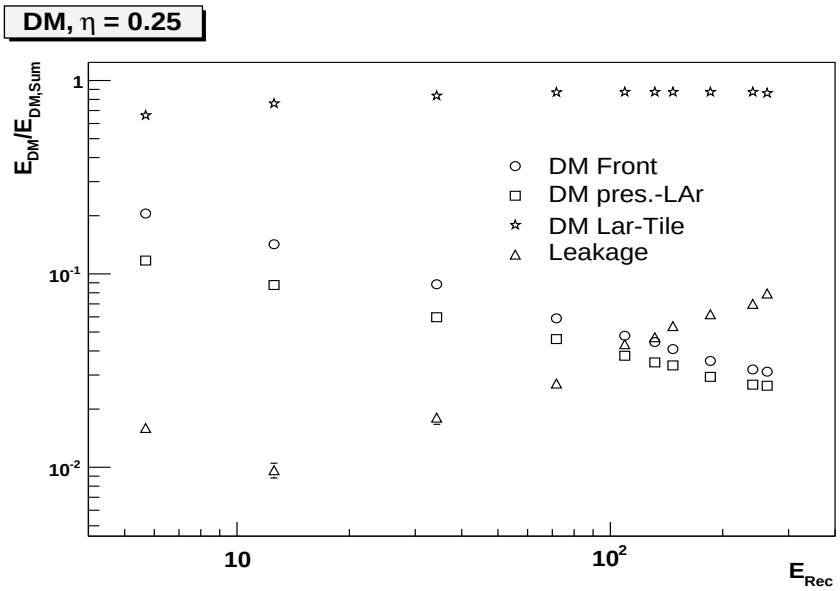

Figure 6: The relative contributions of the various dead material and leakage corrections as a function of beam energy.

deposited by electrons and positrons, non-electromagnetic energy, deposited by charged hadrons, invisible energy, that is gained or lost by breaking up nuclei, and escaped energy, carried out of the cell by a particles, which escape the detector, for example, neutrinos [13]. For each energy and sampling we have constructed profiles of weights $\langle w \rangle = f(\rho)$ with 20 bins.

6 Pion energy reconstruction

6.1 Weights without cut

At the first step we have reconstructed pion energies with weights without any cut. Some examples of these weights at 180 GeV are given in Fig. 7.

These weights have a small relative difference (10% – 45%) for the low and high energy densities in cell. At the same time in the successful H1-method these differences reach 400% [14, 15].

Fig. 8 shows the obtained energy resolution, $\sigma/mean$. The curves are the result of a fit of a quadratic parametrization

$$\sigma/E = a/\sqrt{E} \oplus b \oplus c/E. \qquad (20)$$

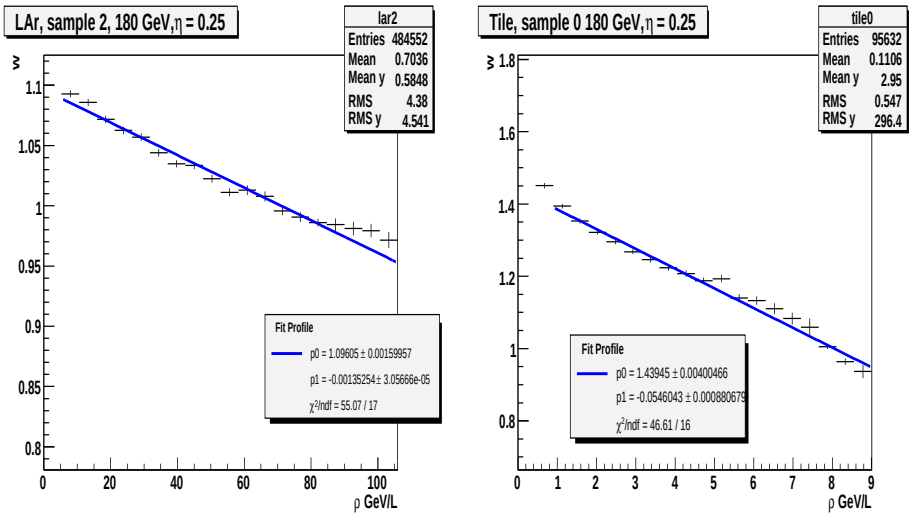

Figure 7: The weights for the LAr_2 and $Tile_0$ samplings at 180 GeV without any cut.

The dashed line is the projected energy resolution (1). It turned out that the experimental energy resolution is about 1.5 times worse than the Monte Carlo simulation and 2 times worse the projected resolution.

The reason of the difference between the experiment and the Monte Carlo simulation could be bigger energy fluctuations in cells in experimental events than in the Monte Carlo events. This can be seen in Fig. 9 where the energy resolutions in electromagnetic scale for the experimental events and the Monte Carlo ones are demonstrated. The significant difference (28% in "a" parameter) is observed.

6.2 Weights with cut

For improving of energy resolution by the enlargement of relative difference between weights for the low and high energy densities in cells and taking into account that our calorimeters are non-compensated ($e/h_{LAr} = 1.74$ [16] and $e/h_{Tile} = 1.36$ [17]), so $e/\pi > 1$, for example, $e/\pi_{LAr} = 1.48$ at 10 GeV. And on cells level $E_{truth} > E_{rec,em}$, therefore $w > 1$, we have introduced the weight cuts (w_{cut}).

We have analysed data with weights $w_i > w_{cut}$ with different cuts of 1, 1.025, 1.05. At this we do not cut the high energy density region

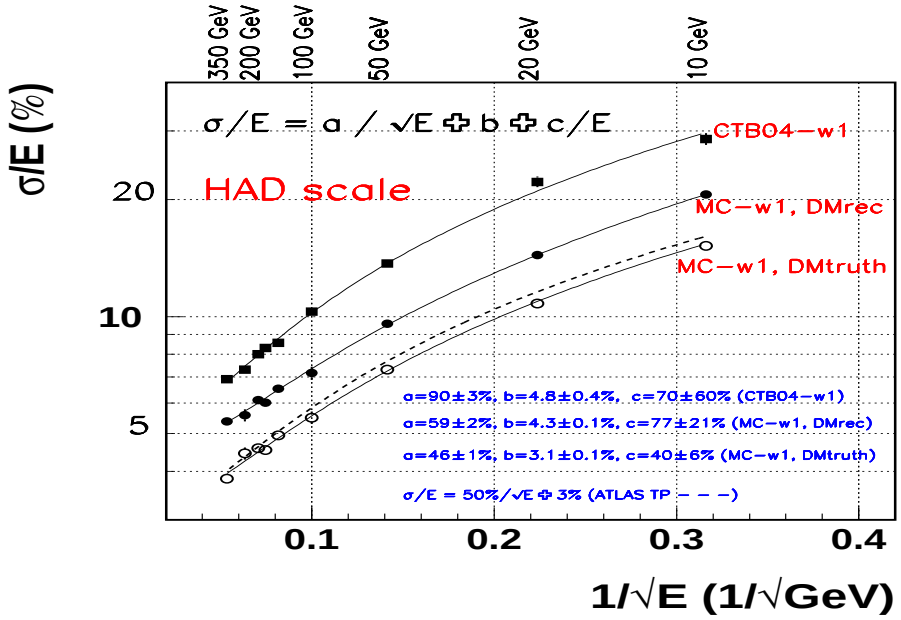

Figure 8: The energy resolution in hadronic scale with the weights without cut (w-1) for the CTB04 data (squares) and the MC simulation (circles). The MC simulation results are with the reconstructed (full circles, DM_{rec}) and true (open circles, DM_{truth}) energy depositions in the dead material between the LAr and Tile calorimeters. The dashed line is the projected resolution (1).

where the electromagnetic energy deposition more than 90%. For this we have determined using figures like Fig. 10 (the electromagnetic fraction as a function of density, the result of the Monte Carlo simulation) for each beam energy and sampling the cell energy densities at which the electromagnetic fraction is more than 90%.

We have investigated the dependence of energy resolution and the mean reconstructed energy from a value of w_{cut} for 180 GeV. The results are presented in Fig. 11.

It can be seen that the energy resolution is improved and the mean energy is increasing with the increasing of w_{cut}. The mean energy is equal to unit for $w_{cut} = 0.7$.

Fig. 12 demonstrates some examples of the weights with $w_{cut} = 1.05$

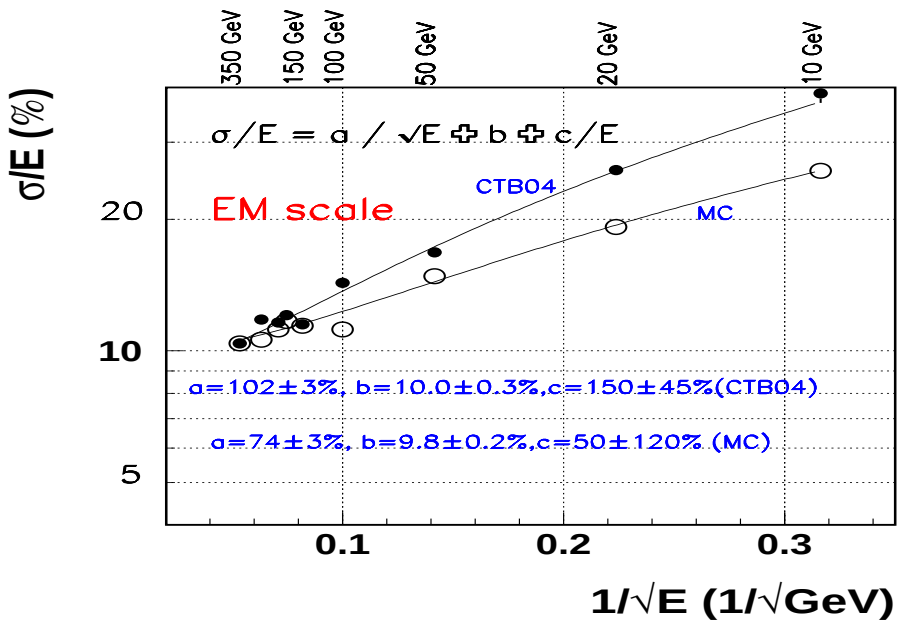

Figure 9: The energy resolution in electromagnetic scale for the CTB04 data (full circles) and the MC simulation (open circles).

(weights w-2). The differences between the values at low and high densities are 70% for LAr_2 sampling and 370% for $Tile_0$ sampling at 100 GeV.

The energy distributions obtained with these weights are shown in Fig. 13. From such distributions the values σ and *mean* have been obtained as a result of Gaussian fit within $\pm 2\sigma$.

Fig. 14 shows the comparison of the experimental and Monte Carlo longitudinal profiles at 100 GeV. One sees that the energy depositions in the LAr samplings for the Monte Carlo are larger than for the experimental events. In order to compensate the difference between the used Monte Carlo and the CTB04, to correct the weights at high density and to improve the energy resolution, we have introduced the additional coefficient, C_{LAr}, to the energy reconstruction formula (2)

$$E_{rec,\ had} = C_{LAr} \cdot E_{LAr} + E_{Tile} + E_{dm} + E_{leak}. \qquad (21)$$

The value of this coefficient of 1.05 have been obtained by minimization of the energy resolution.

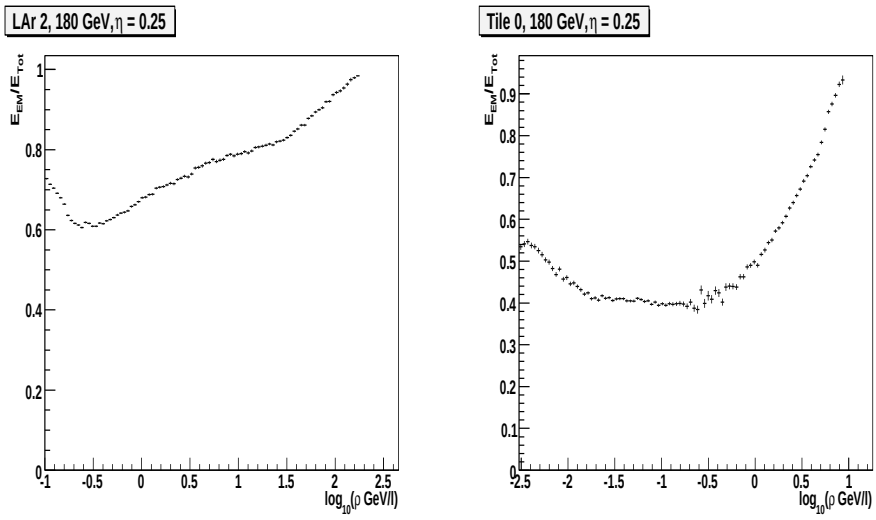

Figure 10: The electromagnetic energy fraction in the LAr_2 sampling (left) and $Tile_0$ (right) at 180 GeV as a function of density obtained by the MC simulation.

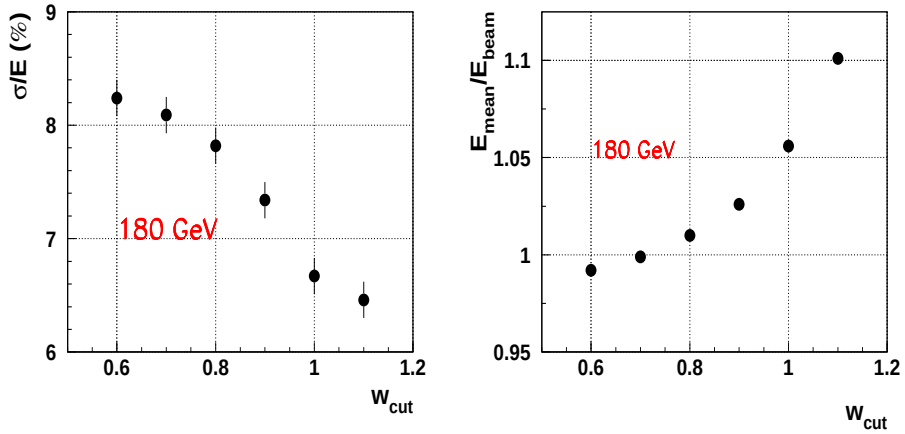

Figure 11: The energy resolution (left) and linearity (right) at 180 GeV as a function of w_{cut}.

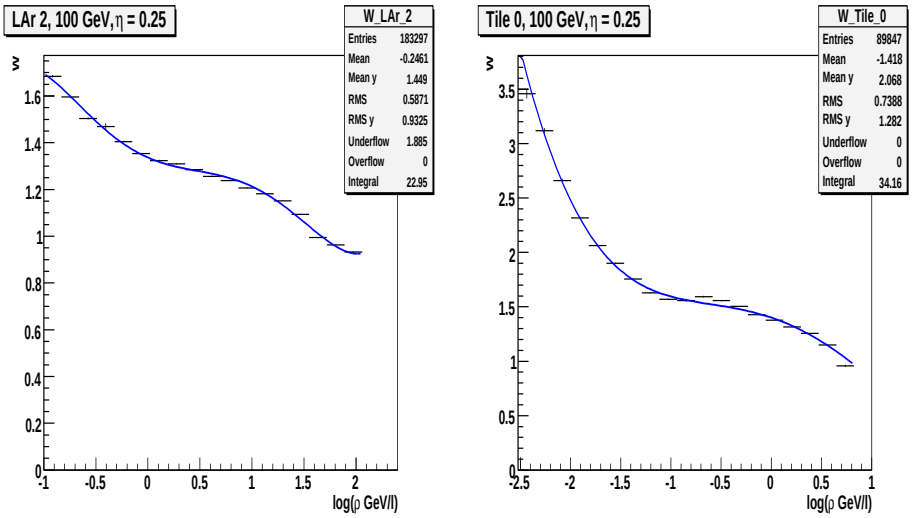

Figure 12: The weights (w-2) with $w_{cut} = 1.05$ for LAr_2 (left) and $Tile_0$ (right) samplings at 100 GeV.

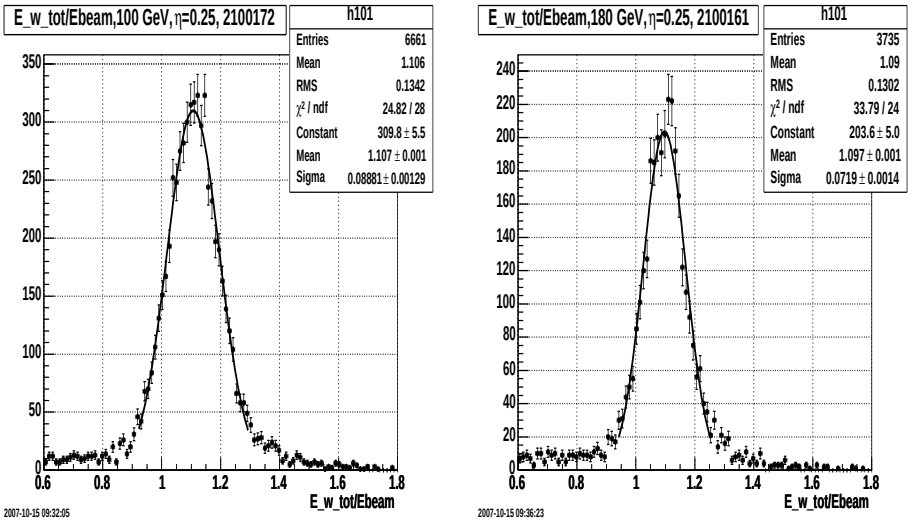

Figure 13: Examples of the energy distributions for $w_{cut} = 1.05$ at 100 GeV (left) and 180 GeV (right).

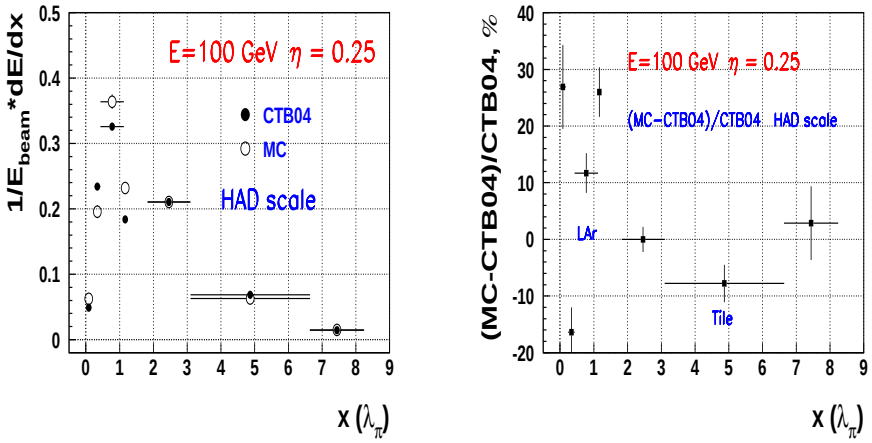

Figure 14: The differential longitudinal energy depositions in hadronic scale at 100 GeV for the CTB04 data and the Monte Carlo simulation (left) and the relative energy depositions ((MC-CTB04)/CTB04) (right).

Fig. 15 shows the energy resolution with and without this correction to energy depositions in the LAr calorimeter. The resolution is increased on 6%.

The linearity for these two cases is shown in Fig. 16. These linearities are within ±1%. The mean value is increased from 1.040 to 1.057.

The experimental energy resolutions for cuts of 0, 1.0, 1.05, $C_{LAr} = 1.05$ and for the Monte Carlo simulation with the $w_{cut} = 1.05$ are shown in Fig. 17. Results of the fit by the function (13) are given in Table 1. The energy resolution is improving with increasing of w_{cut}. The best energy resolution is for $w_{cut} = 1.05$ for which $a = (66 \pm 2)\%$.

Fig. 18 demonstrates the dependencies of "a" and "b" parameters of the energy parametrization (18) from w_{cut}. These parameters are decreasing with increasing of w_{cut}.

Fig. 19 shows the energy linearities for our data with w_{cut} of 1.0 and 1.05. Our energy linearity is mostly within ±1%.

The mean values are given in Table 2. The ones increase with the cut increasing. For $w_{cut} = 1.05$ the mean value is equal 1.093.

We have determined the general normalization constant of 0.91 for

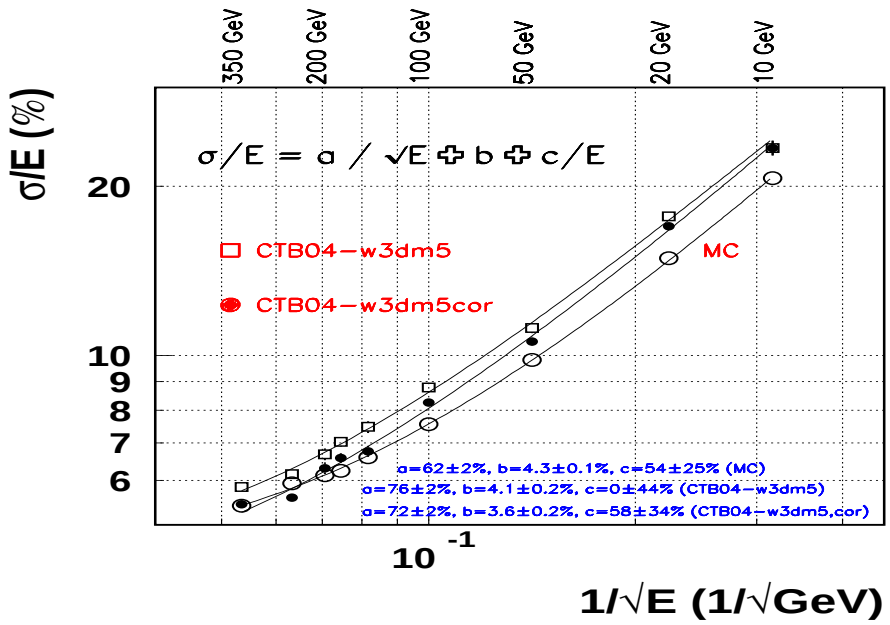

Figure 15: The experimental energy resolution with (full circles) and without (squares) the coefficient C_{LAr} and the Monte Carlo simulation (open circles) with the C_{LAr}.

which the mean value of linearity for $w_{cut} = 1.05$ is about 1. We do not apply this normalization constant to cells with the electromagnetic energy more 90% at high densities. The obtained energy linearity is shown in Fig. 20.

The values of E_{rec}/E_{beam} are within $\pm 1\%$. Fig. 21 demonstrates the energy resolution with and without the general normalization constant. The resolution has not changed.

6.3 Tile Calorimeter signal correction

Recently it has been found out [18] – [21] that the longitudinal samplings $Tile_1$ and $Tile_2$ have been miscalibrated at the cesium calibration due to increasing depth of scintillating tiles with increasing radius of the Tile calorimeter [22].

This is demonstrated in Fig. 22 where the energy response of electrons

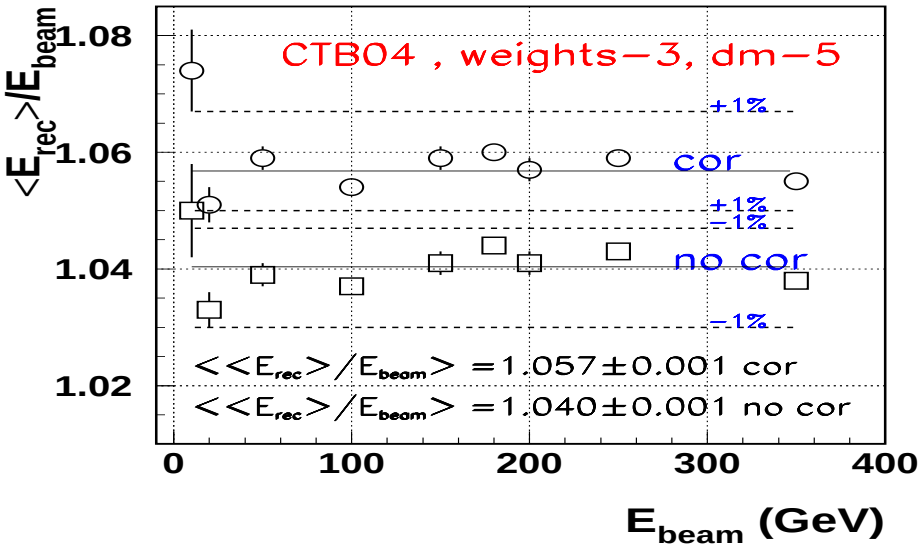

Figure 16: The energy linearity with (circles) and without (squares) of the C_{LAr}.

impinging at $\theta = 90^o$ on TileCal modules as a function of Tilerow number for three barrel modules calibrated in the 2002 – 2003 Testbeam is shown. This response is significantly decreased as Tilerow number is increased.

So, the $Tile_1$ sampling has been undercalibrated by 2.5% and the $Tile_2$ sampling by 4.5%. Corresponding correction of the electromagnetic calibration constants have resulted in improving of the RMS values in distributions of ones from 3.9% to 2.9% (Fig. 23).

We have corrected this undercalibration by multiplying the energy of cells in the $Tile_1$ sampling by factor of 1.025 and in the $Tile_2$ sampling by 1.045. The obtained results for linearity and for energy resolution are shown in Fig. 24. Linearity is good within ±1%, the mean is equal to 1.002±0.002. Due to the TileCal signal correction the mean value increased by about 1%. The energy resolutions with and without these corrections coincide within the errors.

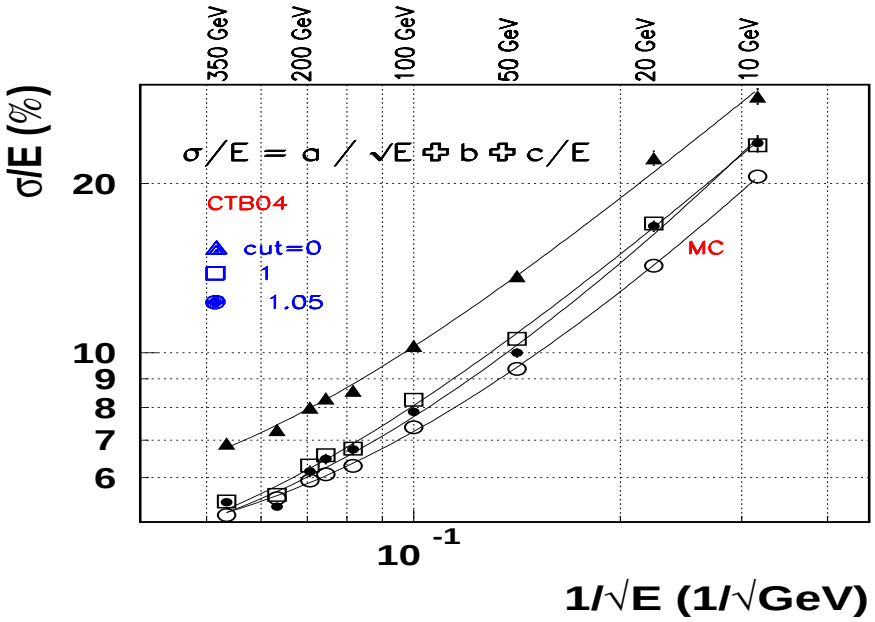

Figure 17: The experimental energy resolutions for several cuts – 0 (triangles), 1.0 (squares), 1.05 (full circles) and for the Monte Carlo simulation with $w_{cut} = 1.05$ (open circles).

Table 1: The parameters of the energy resolution parametrization (20) for various cuts and for the Monte Carlo simulation.

w_{cut}	a (%)	b (%)	c (%)
0	90±3	4.8±0.4	70±60
1.0	72±2	3.6±0.2	58±34
1.025	67±2	3.9±0.2	115±30
1.05	66±2	3.8±0.2	110±20
MC	59±1	4.1±0.1	90±11

Table 2: The mean values of energy linearities for various w_{cut} cuts.

w_{cut}	mean
1.0	1.057±0.001
1.025	1.083±0.002
1.05	1.093±0.003

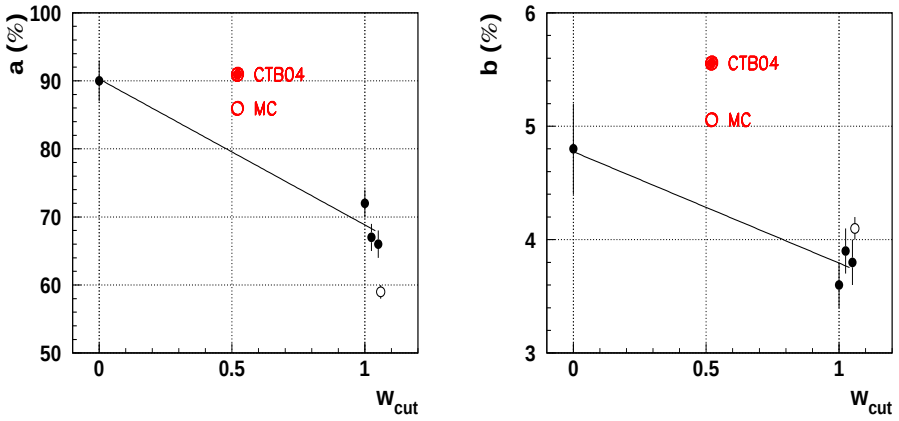

Figure 18: The dependencies of "a" and "b" parameters of the energy parametrization from w_{cut}.

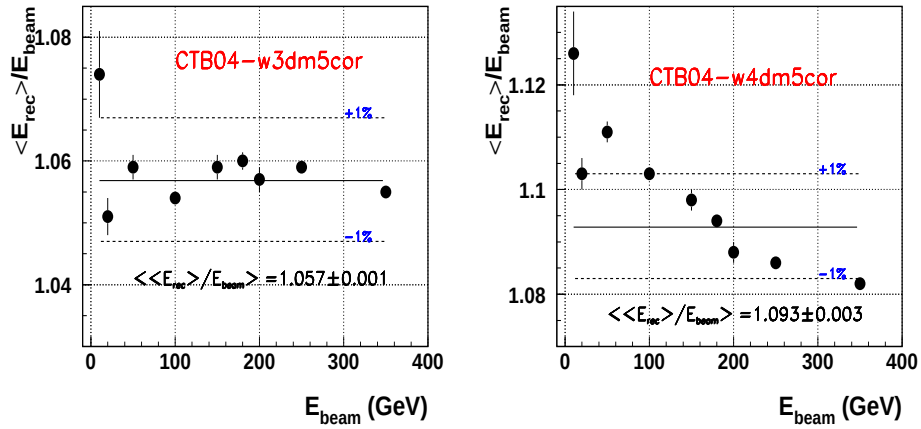

Figure 19: The energy linearities for our data with $w_{cut} = 1.0$ (left) and with $w_{cut} = 1.05$ (right).

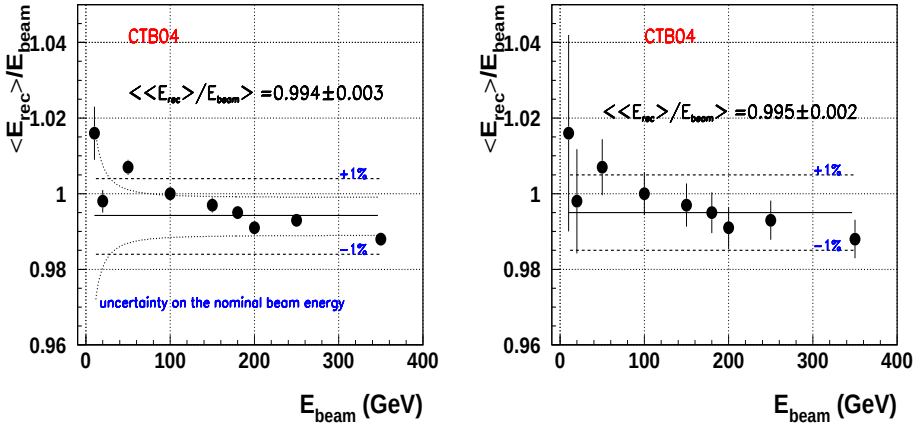

Figure 20: The energy linearity with the general normalization constant: points with only statistical errors (left), points with the quadratically added uncertainties in the nominal beam energies (right).

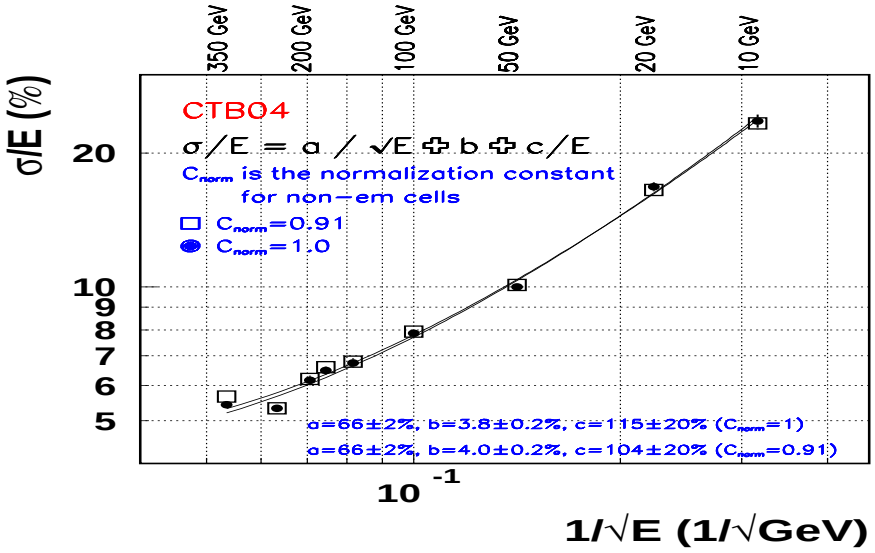

Figure 21: Energy resolution with the general normalization constant (squares) and without normalization (full circles).

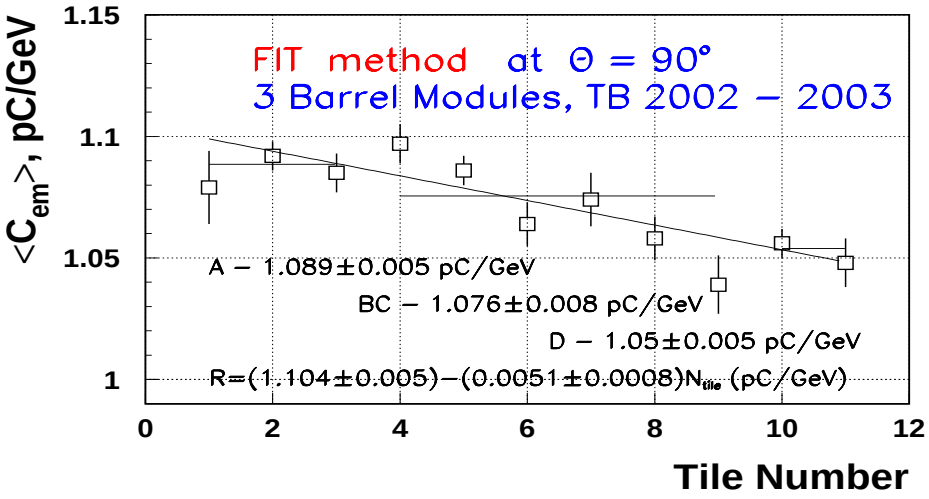

Figure 22: Energy response of electrons impinging at $\theta = 90^0$ on TileCal modules as a function of Tilerow number for three barrel modules calibrated in the 2002 – 2003 Testbeam.

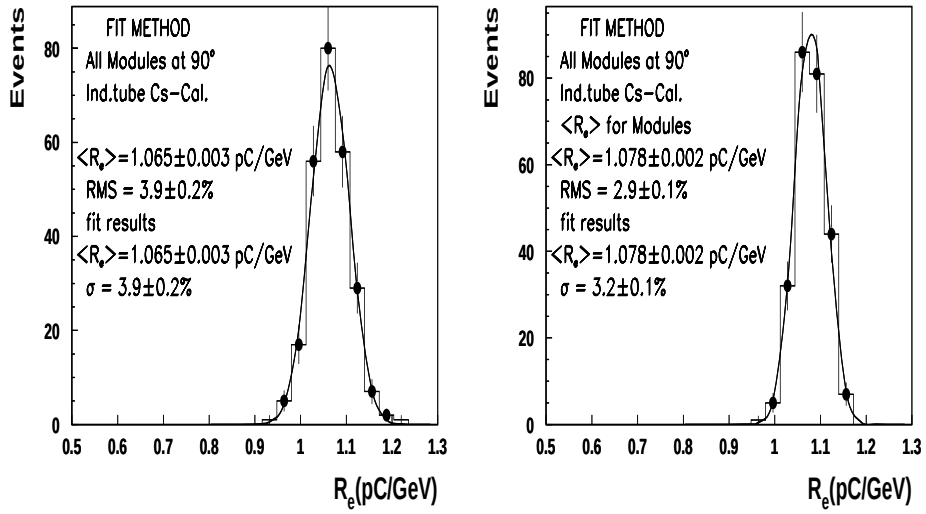

Figure 23: The distributions of the electromagnetic calibration constants without the correction of the $Tile_1$ and $Tile_2$ miscalibration (left) and with this correction (right).

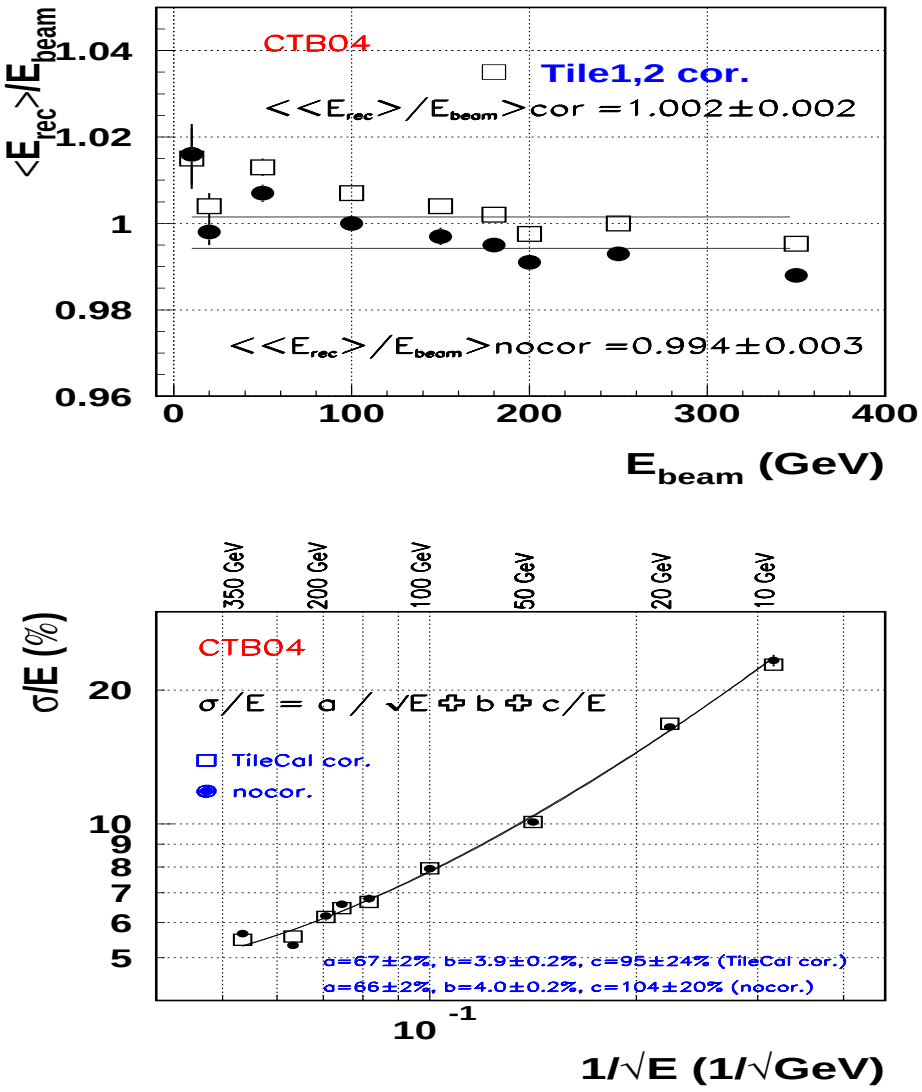

Figure 24: The energy linearity (top) and resolution (bottom) with (squares) and without (circles) the TileCal correction.

6.4 Weighting without knowing of the beam energy

The weights are a function of an incident energy E_{inc} (8). Before we have used $E_{inc} = E_{beam}$. Then we have constructed procedure and TProfile2D(E, ρ, w) for the E_{inc} determination. For each event the total reconstructed energy is determined by 3 steps. The first step is the energy determined by the e/h method [23, 24]:

$$E_{e/h} = (e/\pi)_{LAr} + (e/\pi)_{Tile} E_{Tile} + E_{dm(LAr-Tile)}, \qquad (22)$$

The next two steps are the energies successively determined by the Local Hadronic calibration method.

Weights are extracted from TProfile2D(E_{inc}, ρ, w), containing for 6 samplings 43 logarithmically equidistant beam energies in the range of 3.83 – 501 GeV and 50 bins of logarithm of density for each energy, 10000 simulated events for each energy, release 12.0.8, Physics List QGSP_BERT.

Figs. 25 – 26 show lego plots of these weights (z-axis) for 6 samplings as a function of $\log(\rho)$ (X-axis) and $\log(E_{inc})$ (Y-axis). For the LAr samplings these weights have the values of 1.5 – 1.7 for low densities and of 1 for high densities. For the Tile samplings these weights have the values of 3.7 – 3.5 for low densities. Weak energy dependencies of weights are observed.

Results on energy resolution are shown in Fig. 27.

Without knowing of E_{beam} the degradation of the energy resolution of 9% is observed.

Fig. 28 shows energy linearities with knowing E_{beam} (triangles) and without this knowing (circles), with $C_{norm} = 1$ (top) and with $C_{norm} = 0.966$ (bottom). The linearities are within $\pm 1\%$, the values with and without knowing of E_{beam} coincide. The offset for these weights is of 4%, what is significantly less (9%) then for the w-2 weights.

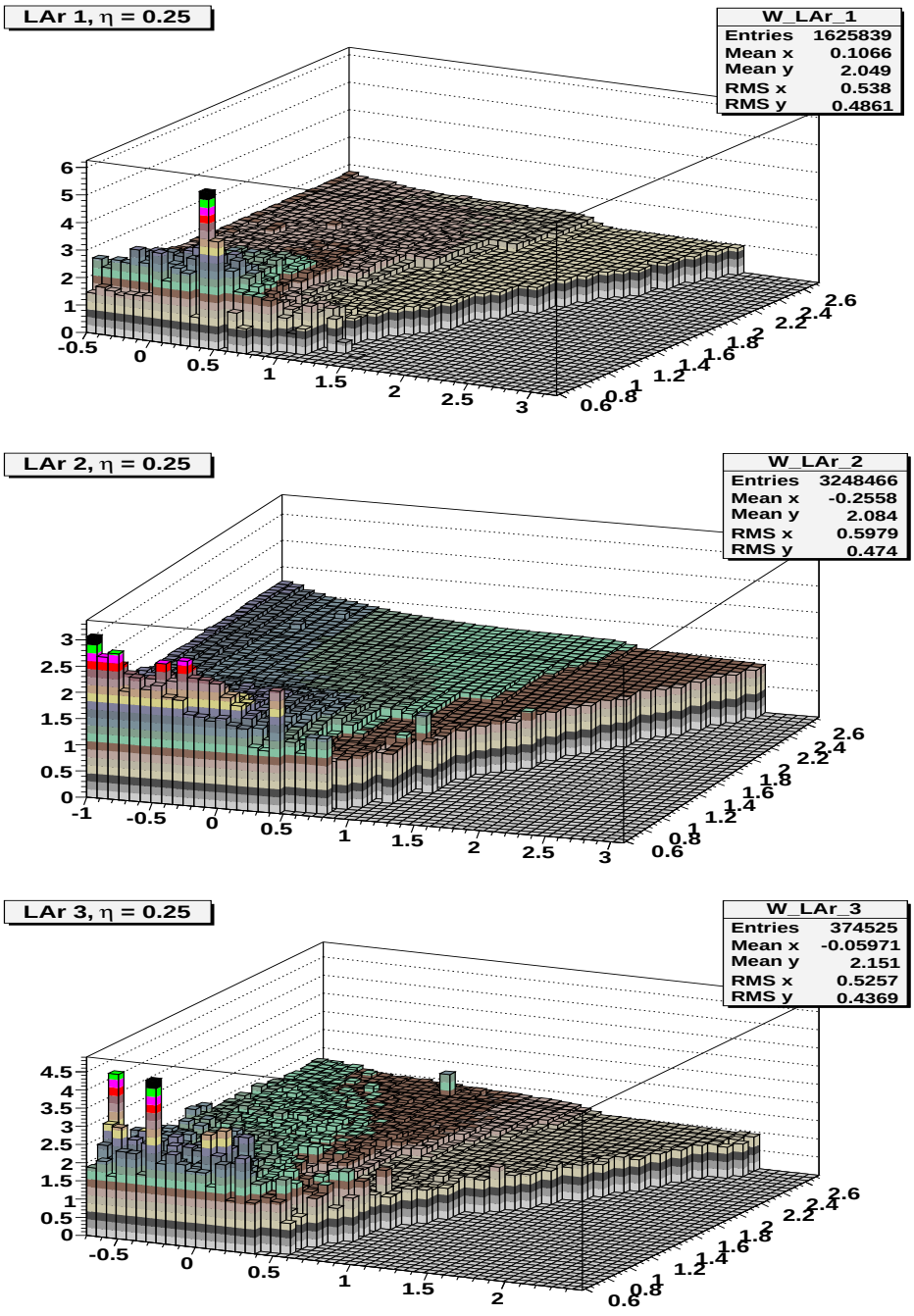

Figure 25: The TProfile2D weights (z-axis) for LAr_1 (top), LAr_2 (middle) and LAr_3 (bottom) samplings as a function of $\log(\rho)$ (X-axis) and $\log(E_{inc})$ (Y-axis).

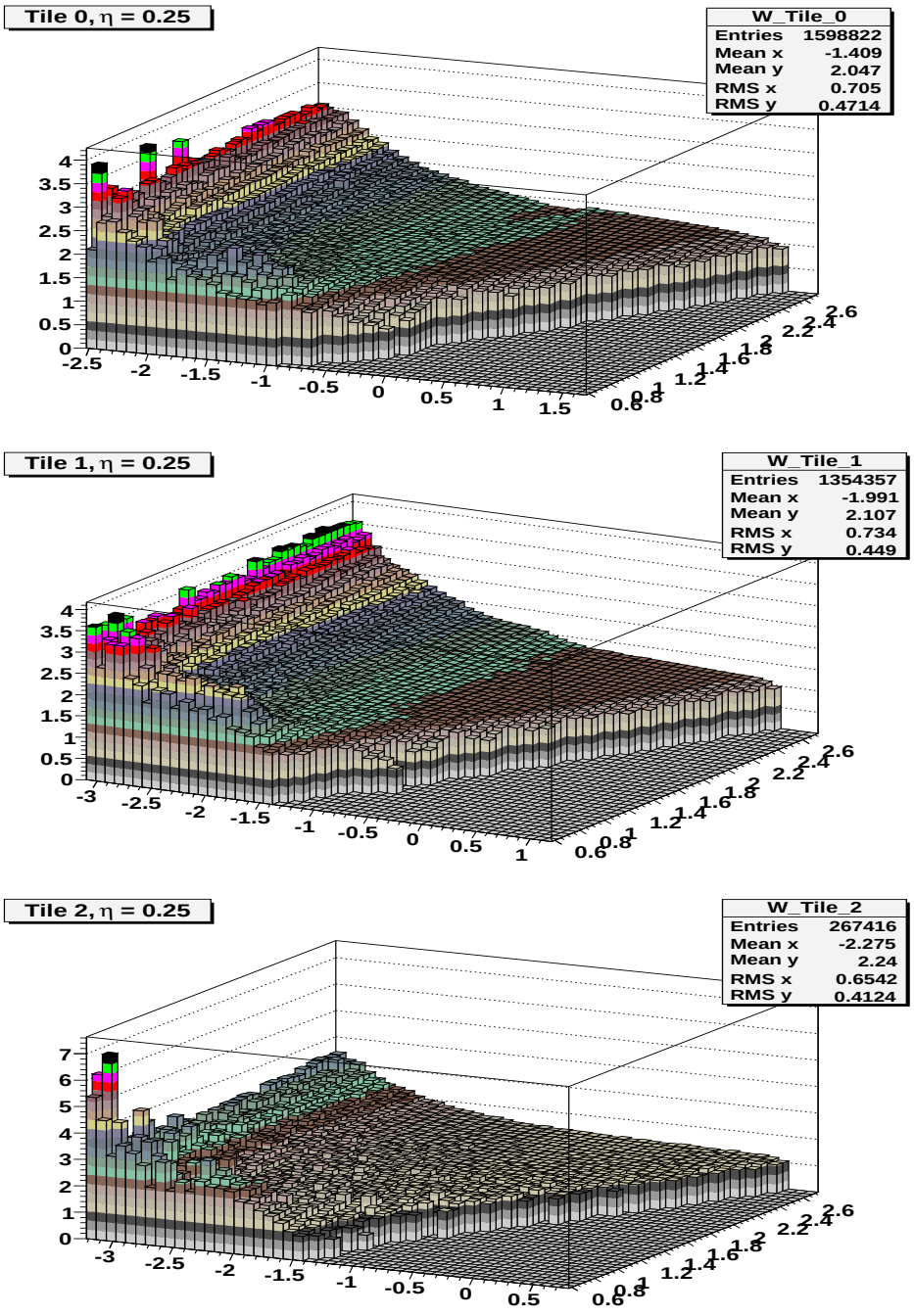

Figure 26: The TProfile2D weights (z-axis) for $Tile_0$ (top), $Tile_1$ (middle) and $Tile_2$ (bottom) samplings as a function of $\log(\rho)$ (X-axis) and $\log(E_{inc})$ (Y-axis).

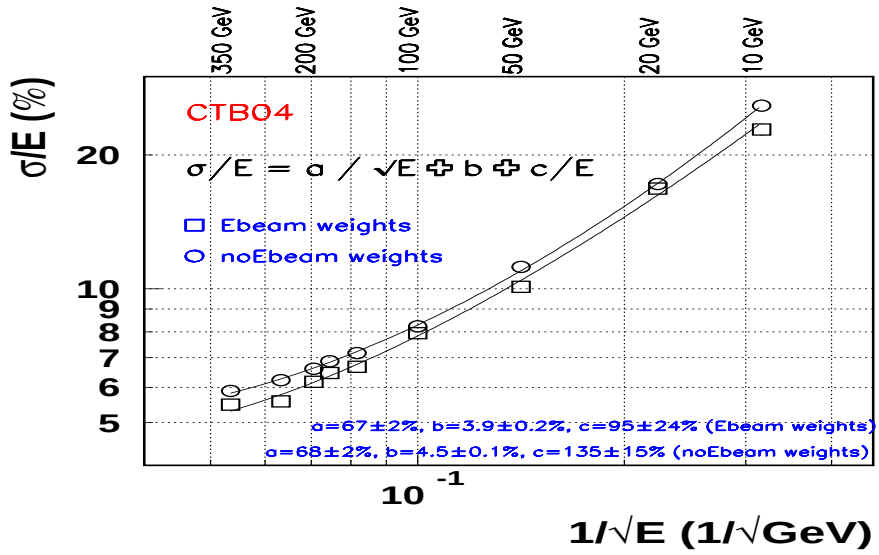

Figure 27: Energy resolution as a function of energy with using of knowing E_{beam} (squares) and without this knowing (circles).

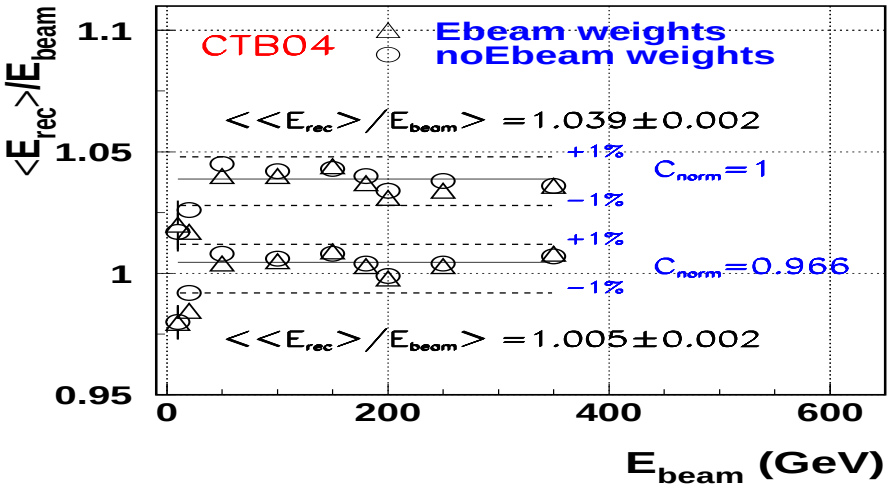

Figure 28: Energy linearities with knowing E_{beam} (triangles) and without this knowing (circles), with $C_{norm} = 1$ (top) and with $C_{norm} = 0.966$ (bottom).

6.5 Comparison with other CTB04 analysis

We have compared the obtained results with the results obtained in [15] and [25]. In [25] the CTB04 data nave been analysed by the Oxford-Stockholm group by the Local Hadronic Calibration method at $\eta = 0.45$ and with weights $w \geq 0.6$. The comparison with our data are given in Fig. 29 (left). Our energy resolution about 1.5 times better than the Oxford-Stockholm group results. Our linearity is within $\pm 1\%$, and the linearity obtained by that group is $\pm 8\%$ (Fig. 29, right). Besides, we have compared in Fig. 29 the Oxford-Stockholm group results with our results (squares) obtained by the e/h method [24]. One sees that these results coincide within the errors.

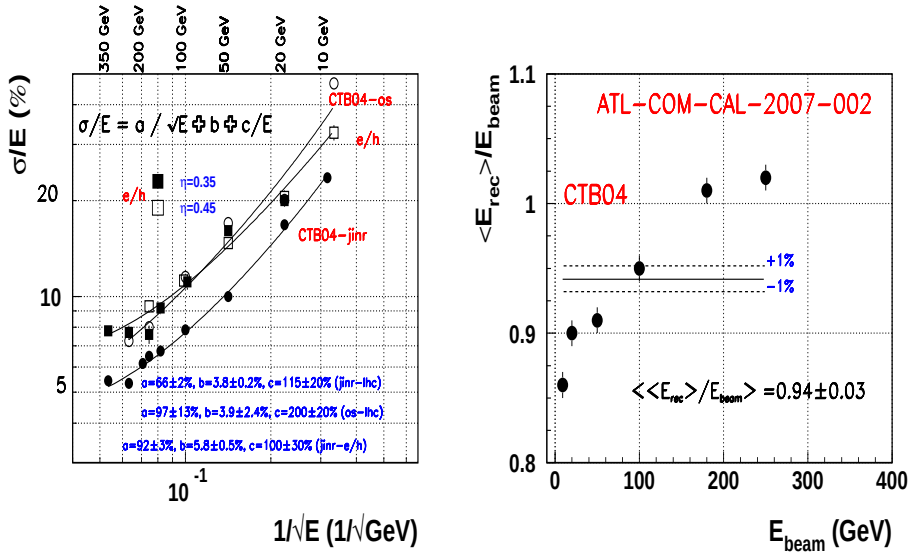

Figure 29: Left: Comparison of our energy resolutions obtained by the lhc method (full circles, this work) and the e/h method (squares) [24] with the results of the Oxford-Stockholm group (open circles) [25]. Right: The energy linearity obtained by the Oxford-Stockholm group [25].

Fig. 30 shows the comparison of our energy resolution with the results of the Pisa group [15] obtained by the H1 method. Our energy resolution slightly better than the H1 method results.

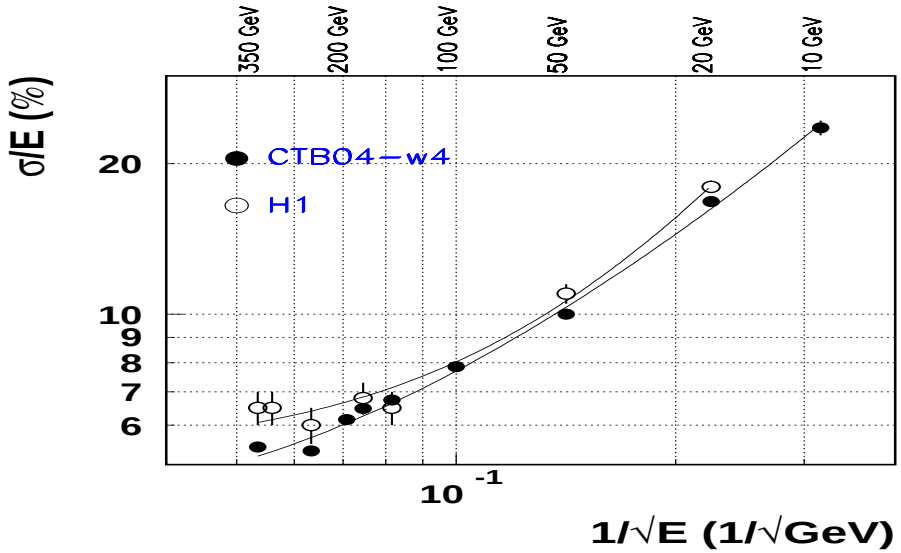

Figure 30: Comparison of our energy resolution (full circles0 with the results of the Pisa group (open circles) [15].

7 Neural Networks application for LAr-Tile dead material energy lost correction

We have applied the Neural Networks for the determination of the energy deposition in the dead material between LAr and Tile [26], [27].

Fig. 31 shows the energy distributions at 250 GeV with the determination of energy deposition in the dead material between LAr-Tile by the conventional method (left) with

$$\sigma/mean = (5.58 \pm 0.08)\%$$

and the Neural Networks method (right) with

$$\sigma/mean = (4.48 \pm 0.06)\%.$$

Improvement is equal to 24%.

Fig. 32 demonstrates the same for 350 GeV. Improvement in this case is equal to 31%.

Energy resolution as a function of energy is shown in Fig. 33. The dashed line is the projected resolution (1), full line is the Monte Carlo

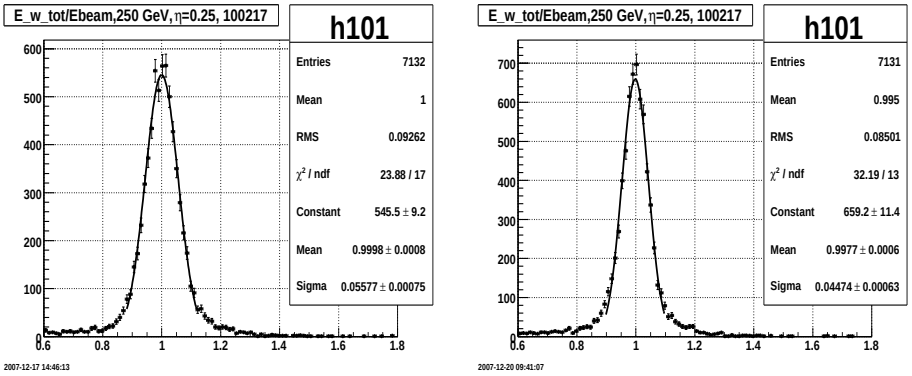

Figure 31: Energy distributions at 250 GeV with the determination of energy deposition in the dead material between LAr-Tile by the conventional method (σ/mean=(5.58±0.08)%) (left) and the Neural Networks method (σ/mean=(4.48±0.06)%) (right).

simulation with the truth dead material energy deposition, squares are the experimental values with the neural networks dead material energy deposition. In this case we have reached the projected resolution (1).

Fig. 34 shows the energy linearity for the experimental data (squares) and the Monte Carlo simulation (circles). It can be seen that the energy

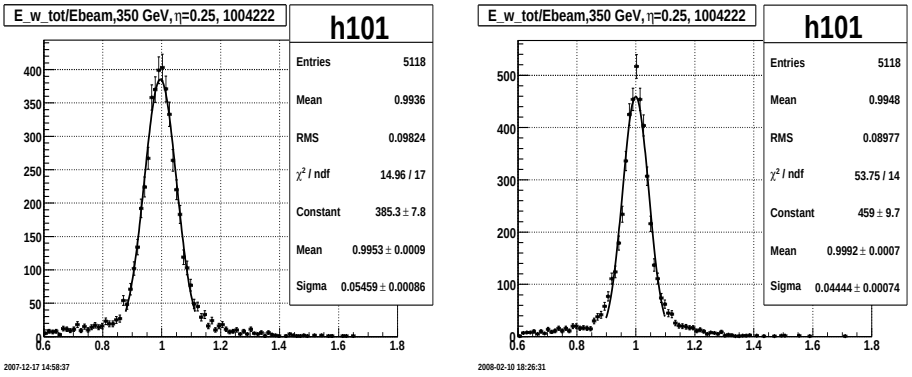

Figure 32: Energy distributions at 350 GeV with the determination of energy deposition in the dead material between LAr-Tile by the conventional method (σ/mean=(5.66±0.09)%) (left) and the Neural Networks method (σ/mean=(4.32±0.07)%) (right).

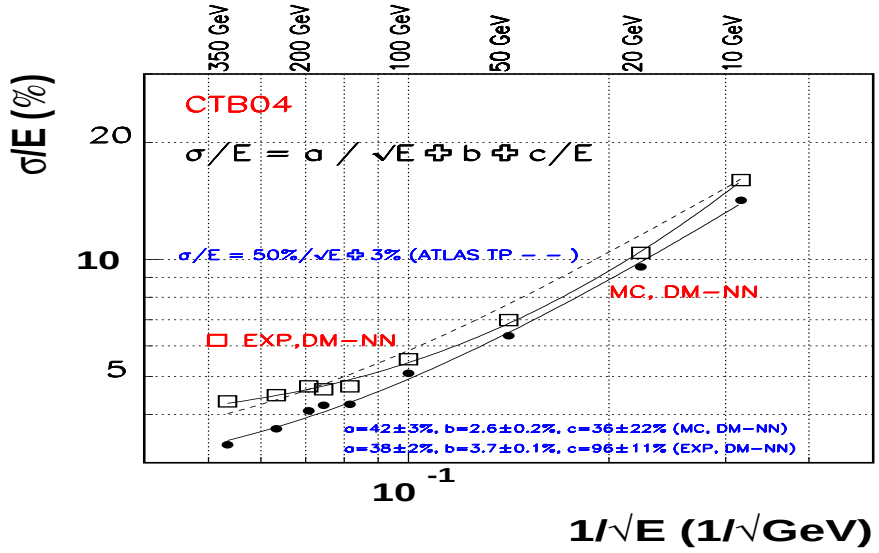

Figure 33: Energy resolution as a function of energy. The dashed line is the projected resolution, full circles are the Monte Carlo simulation with the true dead material energy deposition, squares are the experimental values with the neural networks dead material energy deposition.

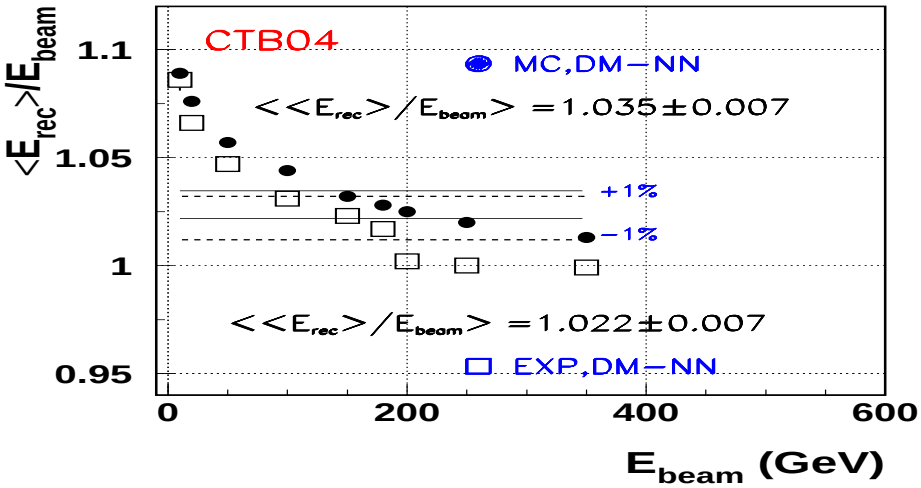

Figure 34: Energy linearity. Full circles are the Monte Carlo simulation with the truth dead material energy deposition, squares are the experimental values with the neural networks dead material energy deposition.

linearity is not sufficiently good.

8 Conclusions

The pion energy reconstruction by the local hadronic calibration method on the basis of the 2004 combined test beam data in the energy range 10 – 350 GeV and $\eta = 0.25$ is performed. In this method energies deposited in each cell are weighted. The weights are determined by the Monte Carlo simulation. We have modified this method by applying cuts in weights. We have investigated various cuts and found out the best ones.

The obtained fractional energy resolution with the conventional method of determination of the energy deposit in the dead material between LAr and Tile calorimeters is

$$\sigma/E = (67 \pm 2)\%/\sqrt{E} \oplus (3.9 \pm 0.2)\% \oplus (95 \pm 22)\%.$$

This is slightly better than the H1 method results for CTB04 obtained by Pisa group and about 1.5 times better than the results for the hadronic calibration method obtained by the Oxford-Stockholm group. The energy linearity is within $\pm 1\%$.

We have determined the general normalization constant of 0.91 for which the mean value linearity for $w_{cut} = 1.05$ is about 1. At using this normalization constant the energy resolution has not worsen.

We have corrected the cesium miscalibration of the $Tile_1$ and $Tile_2$ longitudinal samplings. The mean value of energy linearity has been increased by about 1% and becomes equal to 1.002 ± 0.002. The energy resolution did not change.

We have performed weighting without knowing of the beam energies. For this the special procedure has been developed. In this case the energy resolution shows 9% degradation. Linearities are within $\pm 1\%$, the values with and without knowing E_{beam} coincide. The offset for these weights (release 12.0.8, Physics List QGSP_BERT) is of 4%, what is significantly less (9%) then for the previous weights (release 12.0.6, Physics List QGSP_GN).

The application of the Neural Networks to the determination of the energy deposit between LAr and Tile calorimeters have demonstrated the essential improvement of energy resolution In this case we have reached the projected energy resolution for hadrons in the ATLAS detector $\sigma/E = 50\%/\sqrt{E} \oplus 3\%$.

9 Acknowledgements

This work is the result of the efforts of many people from the ATLAS Collaboration. The authors are greatly indebted to all Collaboration for their test beam setup and data taking. The authors are thankful to J.Budagov, M.Kazarinov and P.Schacht for valuable discussions.

The presented work was partly supported by ISTC Project No. G-1458.

References

[1] ATLAS Collaboration, ATLAS Detector and Physics Performance, Technical Design Report, ATLAS TDR 14, CERN/LHCC/99-14, p.430.

[2] ATLAS Collaboration, ATLAS Detector and Physics Performance, Technical Design Report, ATLAS TDR 15, CERN/LHCC/99-15.

[3] ATLAS Collaboration, ATLAS Technical Proposal, CERN/LHCC/ 94-43, 1994, CERN.

[4] C.Alexa, Y.Kulchitsky, P.Schacht, V.Vinogradov et al., Hadronic Calibration of the ATLAS Calorimeter, https://twiki.cern.ch/ twiki/pub/Atlas/CalorimeterCalibration/hadronic_calibration.doc, 4 July 2003.

[5] B.Di Girolamo et al., Beamline instrumentation in the 2004 combined ATLAS testbeam, ATL-TECH-PUB-2005-001, CERN, Geneva.

[6] C.Issever et al., NIM A545 (2005) 803.

[7] S.Menke, Status of Local Hadron Calibration Weights, Talk given on the Hadronic Calibration Meeting, October 2006, CERN, Geneva.

[8] P.Schaht, Calorimeter hadronic calibration, Talk given on the ATLAS Overview Week, October 2006, CERN, Geneva.

[9] M.Lefebvre, P.Loch, Introduction to Hadronic Calibration in ATLAS, 3 ATLAS Hadronic Calibration Workshop, Milan, Italy, April 2007.

[10] V.Giangiobbe et al., Hadronic calorimeter performance in the ATLAS combined testbeam 2004, ATL-TILECAL-PUB-2005-008, CERN, Geneva.

[11] ATLAS Collaboration, ATLAS Computing Technical Design Report, ATLAS TDR-017, CERN/LHCC/2005-022, 2005, CERN.

[12] S.Menke, Topological Clustering, https://twiki.cern.ch/twiki/bin/view/Atlas/TopologicalClustering

[13] M.Leltchouk, https://twiki.cern.ch/twiki/bin/view/Atlas /CaloSimulation#Simulation_with_Calibration_Hits

[14] M.P.Casado, M.Cavalli-Sforza, H1-inspired analysis of the 1994 combined test of the Liquid Argon and Tilecal calorimeter prototypes, ATL-TILECAL-96-075, CERN, Geneva

[15] C.Roda, I.Vivarelli, Cell Based Jet Calibration, ATL-PHYS-PUB-2005-019, CERN, Geneva.

[16] Y.Kulchitsky, M.Kuzmin, V.Vinogradov, Non-compensation of an Electromagnetic Compartment of a Combined Calorimeter, ATL-TILECAL-99-021, CERN, Geneva

[17] J.Budagov, Y.Kulchitsky, V.Kuzmin, V.Vinogradov, The e/h ratio of the ATLAS Hadronic Tile Calorimeter, ATL-TILECAL-2001-001, CERN, Geneva.

[18] A.Henriques, Y.Kulchitsky, Electron calibration at 90 deg. versus a tile number, Talk given on the TileCal Pion Taskforce Meeting, 23 May 2007, CERN, Geneva.

[19] A.Henriques, Y.Kulchitsky, Update of electron/Cs using true beam energy, Talk given on the TileCal Pion Taskforce Meeting, 17 October 2007, CERN, Geneva.

[20] A.Henriques, Y.Kulchitsky, Study of Electron response at 90 degrees on July 2002 new data; Talk given on the Tilecal Pion Taskforce meeting of ATLAS Collaboration, 06.02.2008, CERN, Geneva, Switzerland.

[21] A.Henriques, Y.Kulchitsky, Some "almost final" conclusions on Electron analysis with new ntuples; Talk given on the Tilecal Pion Taskforce meeting of ATLAS Collaboration, 05.03.2008, CERN, Geneva, Switzerland.

[22] ATLAS Collaboration, ATLAS Tile Calorimeter Technical Design Report, ATLAS TDR 3, CERN/LHCC/96-42, 1996, CERN.

[23] Y.Kulchitsky, V.Vinogradov, NIM A502, 708, 2003.

[24] Y.Kulchitsky, V.Vinogradov, Pion Energy Reconstruction by the e/h method (Combined 2004 Test Beam Data), Talk given on the Hadronic Calibration Meeting, 6 May 2005, CERN, Geneva.

[25] E.Bergeaas et al., Local Hadronic Calibration of Single Pion Data from the Combined ATLAS Testbeam of 2004, ATL-CAL-PUB-2007-001, CERN, Geneva.

[26] Y.Kulchitsky, V.N.Shigaev, P.Tsiareshka, Application of artificial neural networks to reconstruction of the energy lost in LAr/Tile dead material, Talk given on the Hadronic Calibration Meeting, October 2007, CERN, Geneva.

[27] J.A.Budagov, J.I.Khubua, Y.A.Kulchitsky et al., Artificial Neural Networks for reconstruction of energy losses in dead materials between barrel LAr and Tile calorimeters: exploratio and results, ATL-TILECAL-PUB-2008-006, ATL-COM-TILECAL-2008-002, CERN, Geneva.